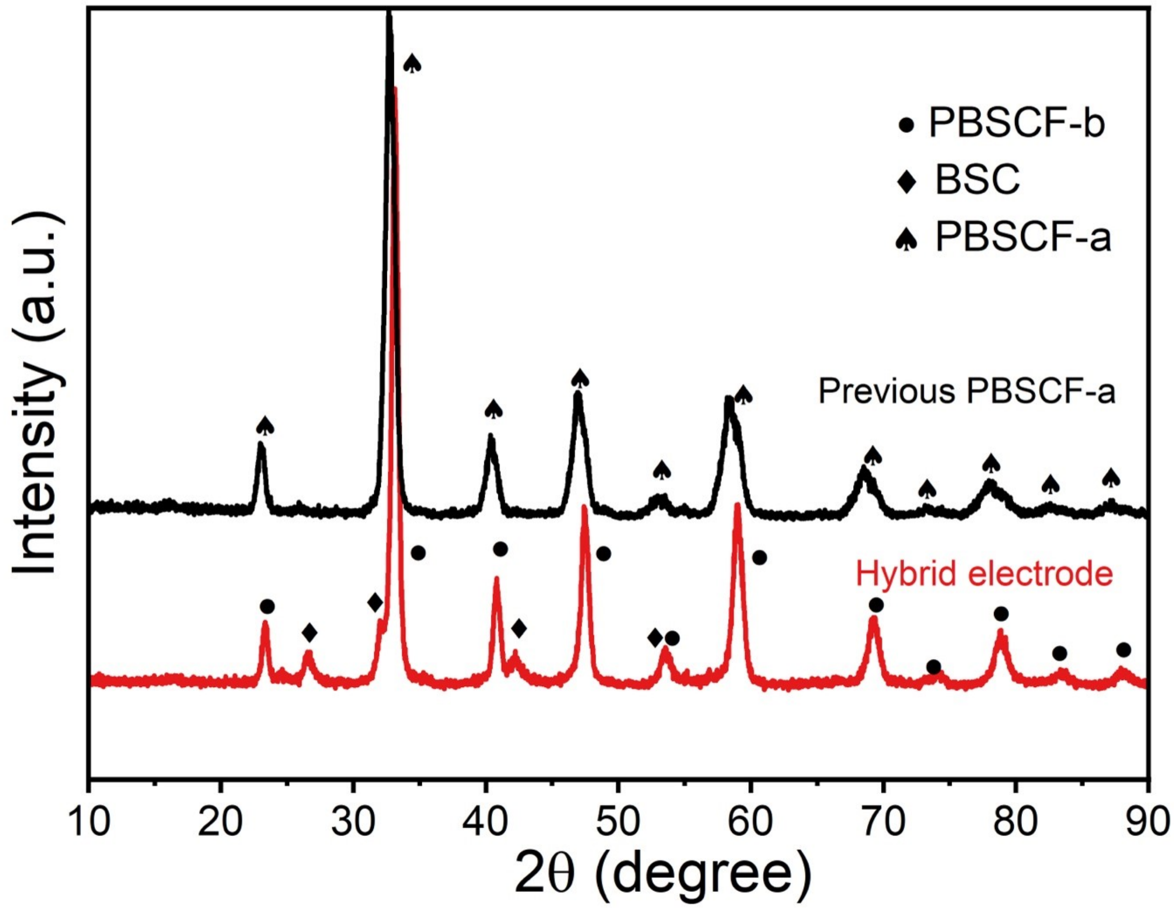

Figure S1. XRD patterns of the previous PBSCF-a phase and the hybrid electrode. The previous PBSCF-a is a single-phase double perovskite, which was synthesized by a wet chemistry method and sintered at 900 °C for 5 hours. The hybrid electrode consists of two phases, PBSCF-b and BSC, which was prepared by the same wet chemistry method and sintered at 750-770 °C.

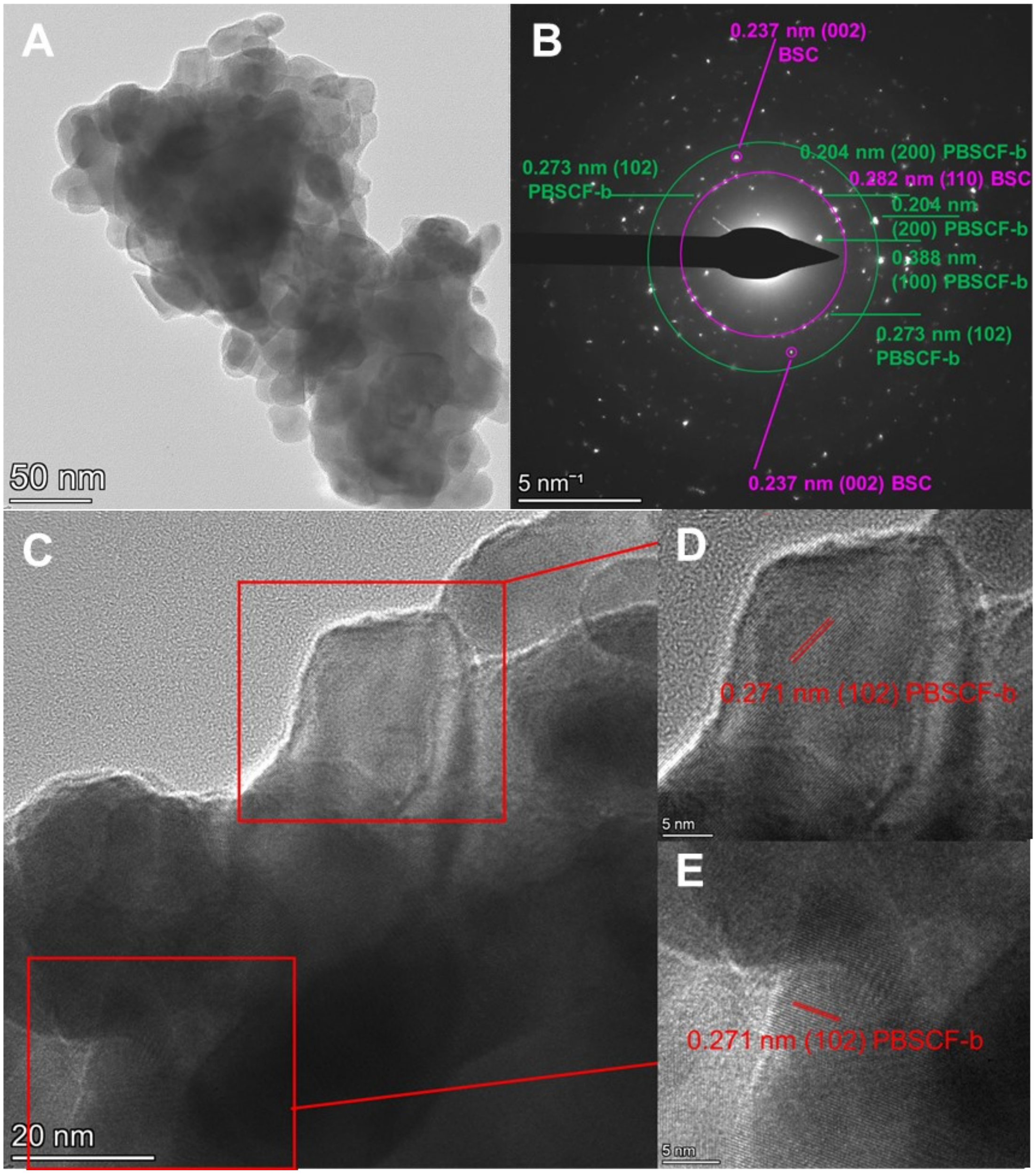

Figure S2. (A) TEM images of the hybrid electrode. (B) SAED patterns indicate the hybrid electrode is composed of the PBSCF-b phase and BSC phase. (C) HR-TEM image of the hybrid electrode grain and the zoomed-in areas: (D) and (E). The lattice fringes with the d-spacing of 0.271 nm, correspond to the (102) planes of the new PBSCF-b phase.

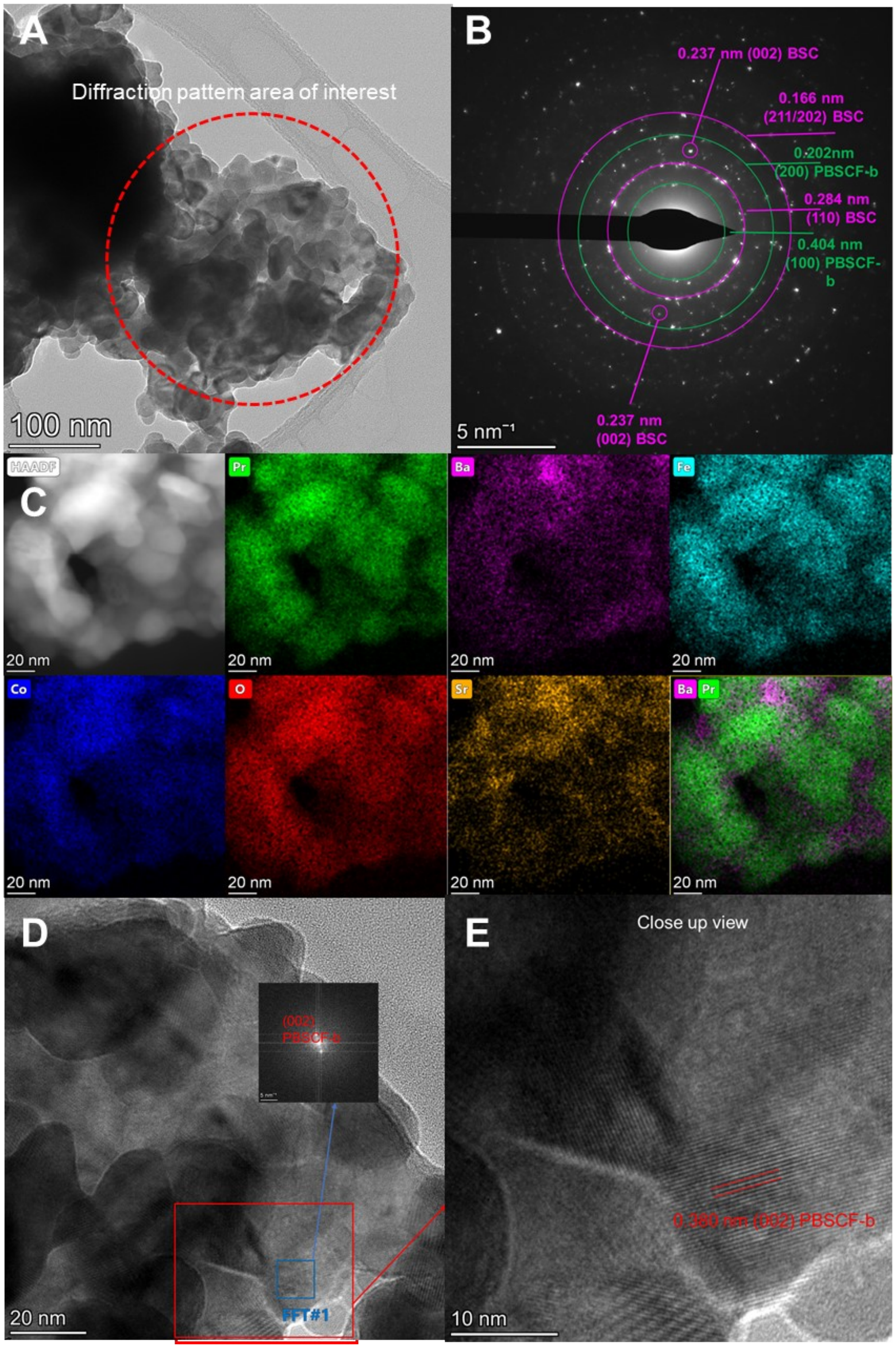

Figure S3. (A) Additional TEM images of the hybrid electrode. (B) Additional SAED patterns show the hybrid electrode is composed of a new PBSCF-b phase and the BSC phase. (C) EDS mapping images of the hybrid electrode show the BSC phase mainly contains Ba, Sr, Co, and O elements. (D) HR-TEM image of the hybrid electrode grain and the zoomed-in areas. (E) HR-TEM image shows lattice planes with d-spacing of 0.380 nm, corresponding to the (002) planes of the new PBSCF-b phase.

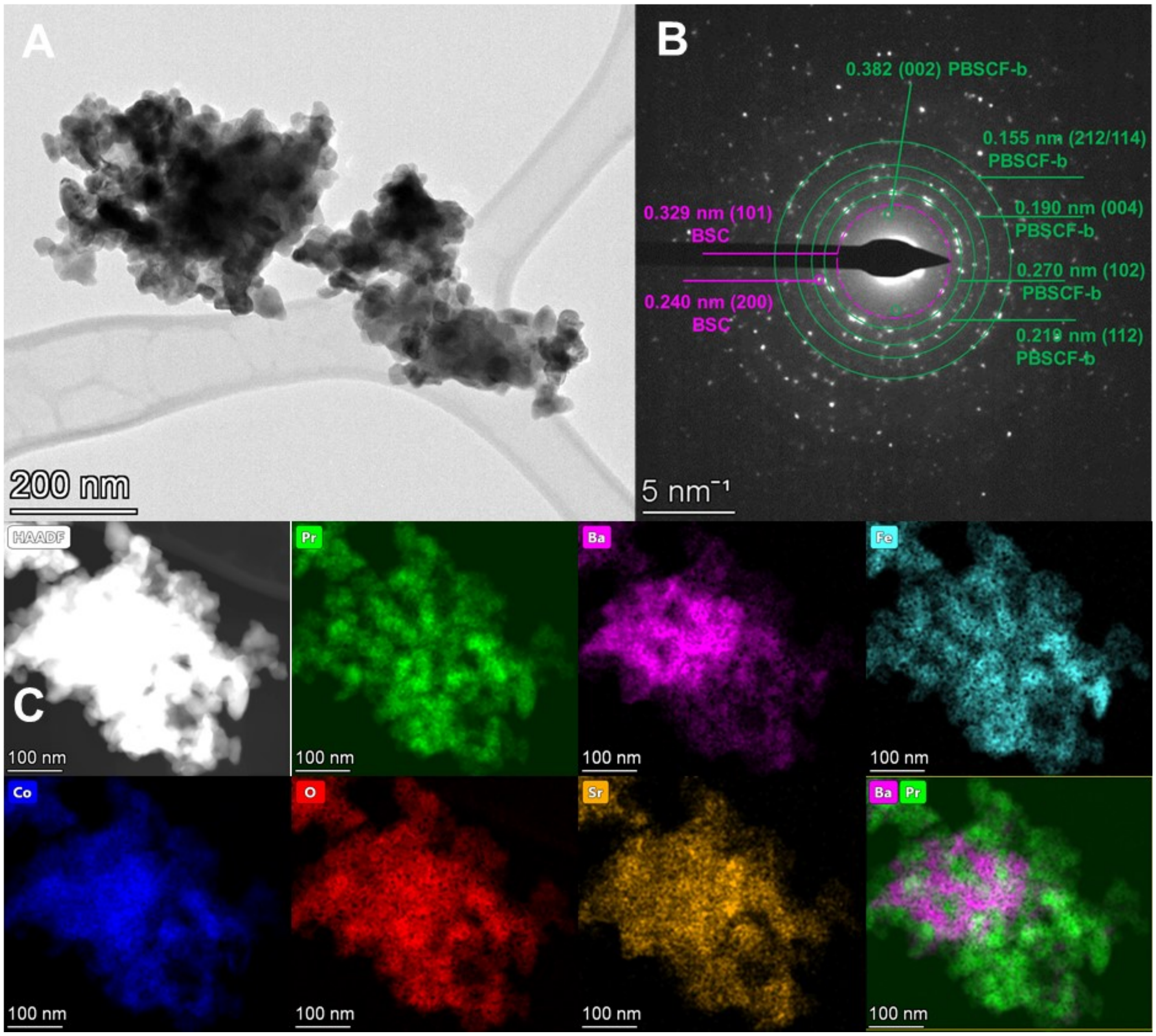

Figure S4. (A) TEM image of the hybrid electrode. (B) SAED patterns show the lattices with the d-spacings of 0.382 nm, 0.155 nm, 0.190 nm, 0.270 nm, and 0.219 nm, corresponding to the (002), (212/114), (004), (102/110), and (112) planes of PBSCF-b, respectively. And those with the d-spacing of 0.329 nm and 0.240 nm correspond to the (101) and (200) planes of BSC, respectively. (C) EDS mapping images of the hybrid electrode confirm that it is a composite of PBSCF-b and BSC phases.

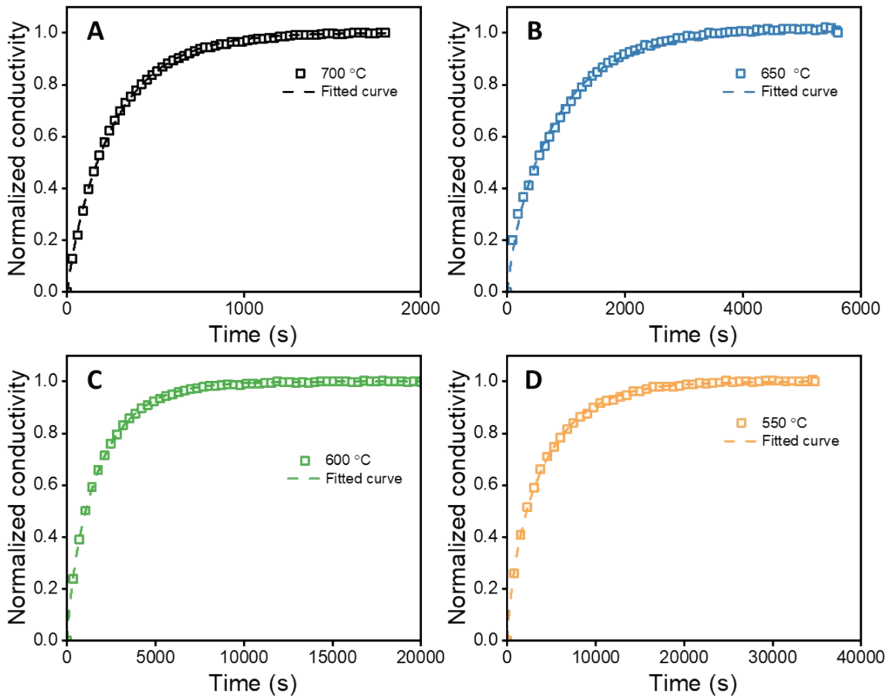

Figure S5. ECR experimental results and the fitted results for PBSCF-b coated with BSC at 550 °C, 600 °C, 650 °C, and 700 °C after changing the oxygen partial pressure from 2 vol.% (490 sccm Ar + 10 sccm O_2) to 20 vol.% (400 sccm Ar + 100 sccm O_2).

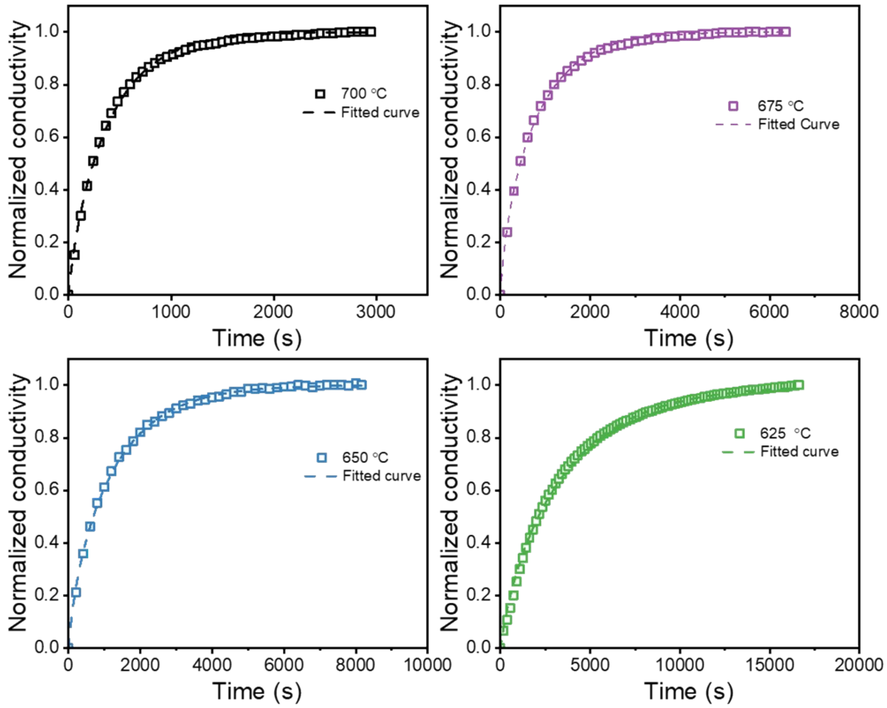

Figure S6. ECR experimental results and the fitted results for the previous PBSCF-a at 625 °C, 650 °C, 675 °C, and 700 °C after changing the oxygen partial pressure from 2 vol.% (490 sccm Ar + 10 sccm O_2) to 20 vol.% (400 sccm Ar + 100 sccm O_2).

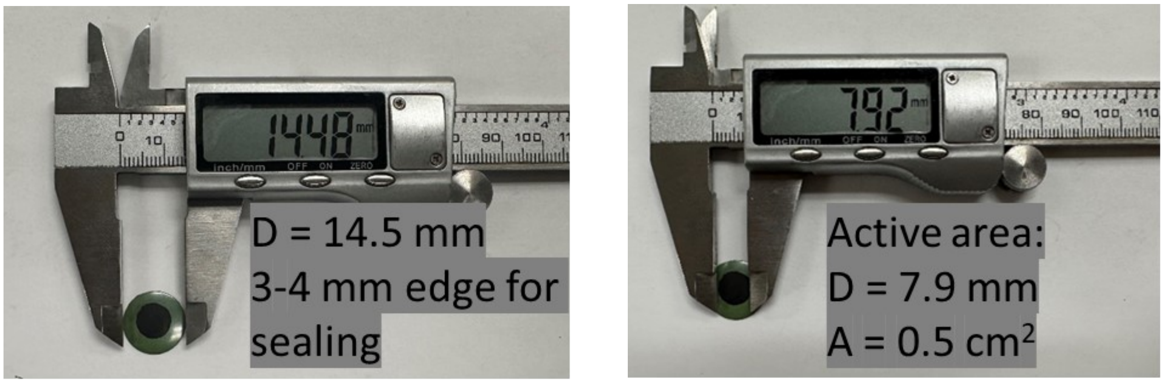

Figure S7. Photos of a representative fuel electrode-supported SOEC fabricated in this work to evaluate the oxygen electrodes. The oxygen electrode effective area is 0.5 cm^2.

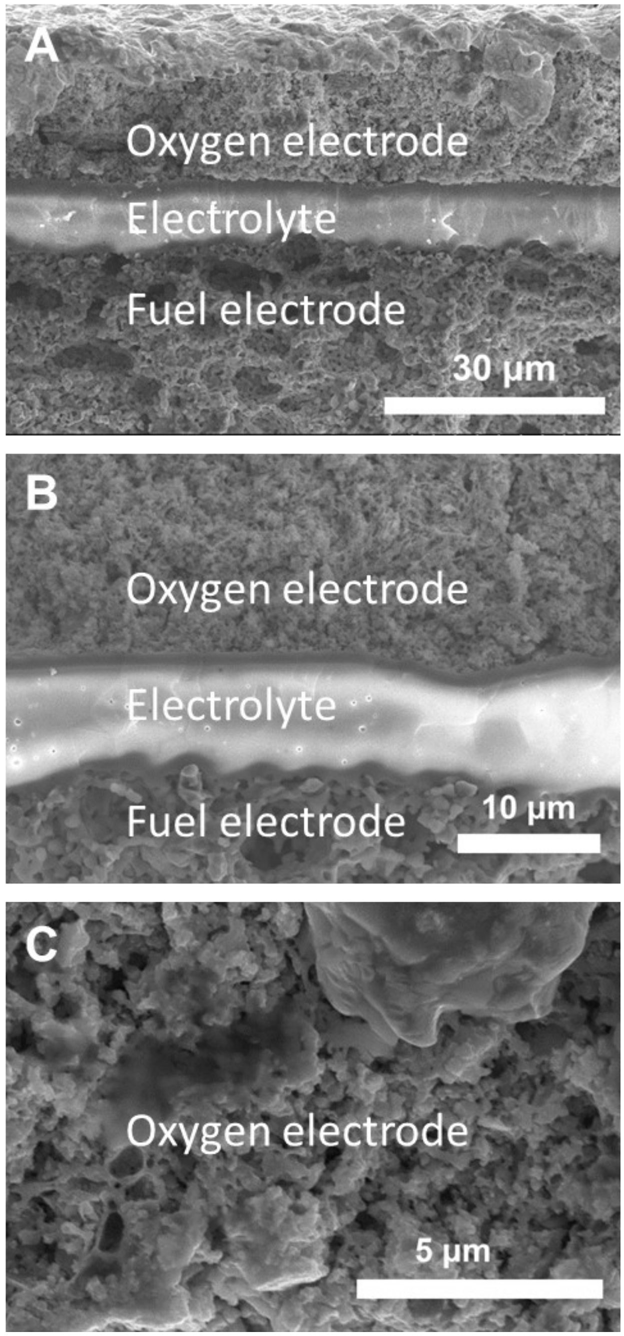

Figure S8. Representative SEM images of SOECs studied in this work, which are highly reproducible, highly uniform, and defect-free, and have dense electrolytes (thickness of electrolyte = ~8 μm).

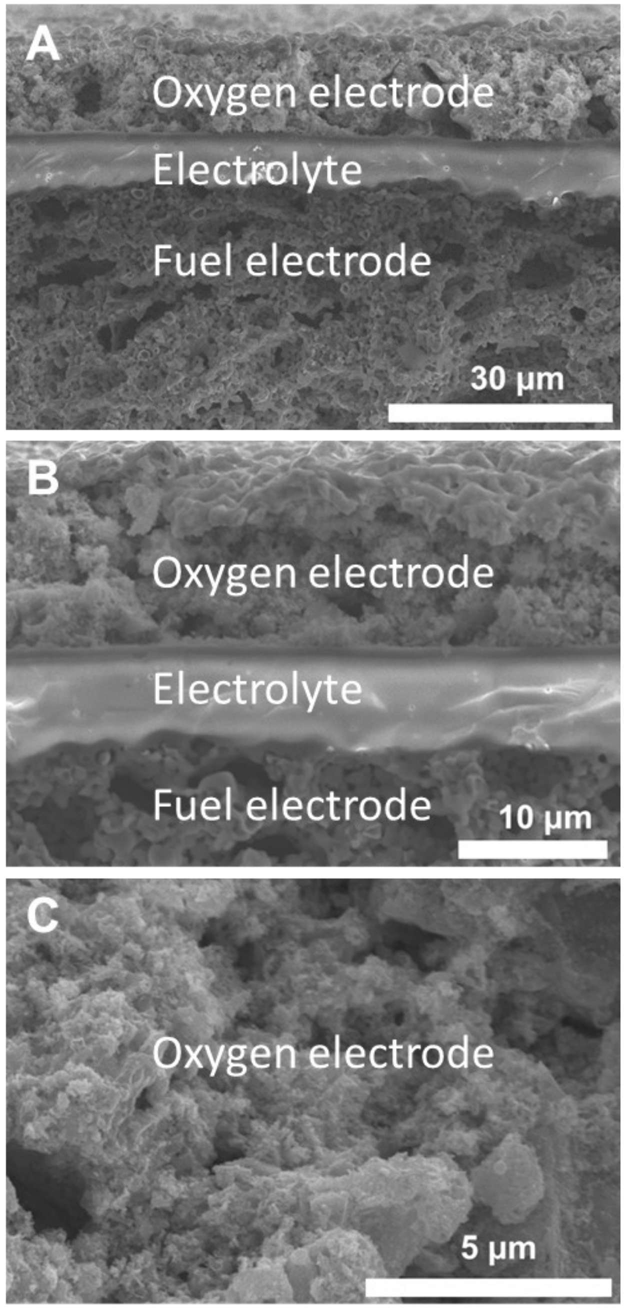

Figure S9. SEM images of the SOEC with PBSCF-b+BSC hybrid electrode after performance evaluation in steam electrolysis mode. No cracking or electrolyte-electrode delamination were observed.

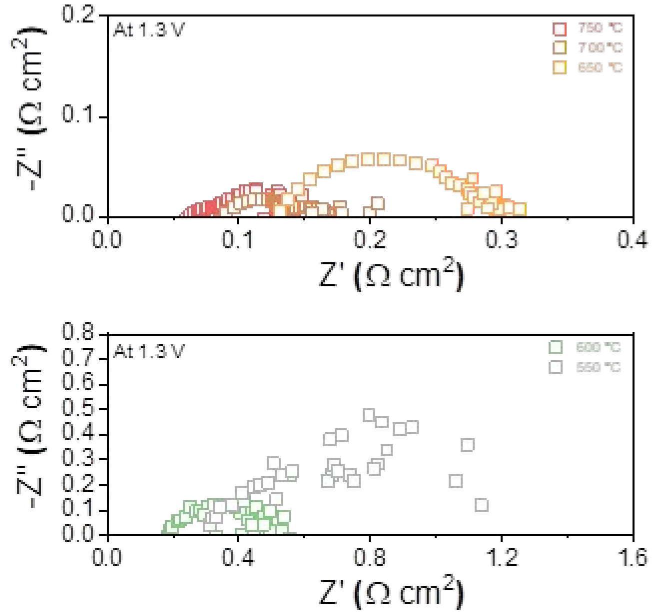

Figure S10. EIS spectra collected at an applied voltage of 1.3 V and an operating temperature ranging from 550 to 750 °C for SOEC with the hybrid electrode.

Table S1. Comparisons YSZ electrolyte-based SOEC performance.

Half-cell configuration	Oxygen electrode materials	Temperature (°C)	Current densities at 1.3 V (A cm^{-2})	Literature
Ni-YSZ|YSZ	Hybrid electrode	750	4.4	This work
		700	2.3	
		650	1.4	
		600	0.9	
		550	0.46	
Ni-YSZ|YSZ|GDC	SSC-SDC	800	4.08	1
		750	3.13	
		700	1.9	
		650	1.1	
Ni-YSZ|YSZ|GDC	STFC	800	3	2
		750	2.3	
		700	1.5	
		650	1	
		600	0.6	
LSCFN55|YSZ	SSNC	800	0.7	3
		750	0.45	
430L|YSZ|SSZ	SSZ-Nd_2O_3/NNO	800	2.05	4
		750	1.62	
		700	1.06	
		650	0.6	
Ni-YSZ|Ni-SSZ|SSZ|SNDC	PBSCF-GDC	750	2.1	5
		700	1.45	
		650	0.94	
		600	0.51	
Ni-YSZ|YSZ	LSM-DYSB	700	1.32	6
		650	0.9	
		600	0.47	
Ni-YSZ|YSZ|SNDC	LSCF-SNDC	750	1.37	7
		700	0.97	
		650	0.58	
Ni-YSZ|YSZ|GDC	LSCF-GDC	800	2.75	8
		750	1.7	
		700	1.25	
		650	0.6	
Ni-YSZ|YSZ	LSM-YSB	800	1.52	9
		750	0.97	
		700	0.7	
		650	0.46	
Ni-YSZ|YSZ|GDC	STFC-PrOx	800	4.25	10
		750	3.6	

		700	2.9	
		650	2.25	
		600	1.25	
		550	0.5	
Ni-YSZ|YSZ|GDC	PBFZr-GDC	700	2.14	11
Ni-YSZ|YSZ|GDC	LSCF-GDC	750	2.1	12
Ni-YSZ|YSZ|GDC	PBNF0.1	750	0.65	13
Ni-YSZ|YSZ	PBSM3	750	2.75	14
		700	1.85	
Ni-YSZ|YSZ	LSM-YSZ	700	0.40	15
Ni-YSZ|YSZ|GDC	LSCF	700	0.82	16
Ni-YSZ|YSZ	LSCF-YSZ	750	0.91	17
Ni-YSZ|YSZ|SDC	BSCF-SDC	750	0.23	18
Ni-YSZ|YSZ	PNO	700	0.28	19
Ni-YSZ|YSZ|GDC	LSCF-GDC	750	0.34	20
Ni-YSZ|YSZ|GDC	LSCF-GDC	750	0.77	21
Ni-YSZ|ScSZ	Mn1.3Co1.3Cu0.4O4-ScSZ	750	1.4	22
Ni-YSZ|YSZ|GDC	LSFN-GDC	750	0.53	23
Ni-YSZ|YSZ|GDC	BCO-PBCC	750	1.36	24

Table S2. Performance comparison of this work and other state-of-the-art YSZ anode-supported hydrogen-fueled SOFCs reported recently.

Half-cell configuration	Oxygen electrode materials	Peak power density at 750 °C (W cm^{-2})	Literature
Ni-YSZ|YSZ	Hybrid electrode	2.4	This work
Ni-YSZ|YSZ|GDC	STFC	1.75	[2]
Ni-YSZ|YSZ|GDC	STFC-PrO_x	3	[10]
Ni-YSZ|YSZ|GDC	LSCF-GDC-PrO_x	2	[25]
Ni-YSZ|YSZ	LSCF-GDC	1.6	[26]
Ni-YSZ|YSZ|GDC	LSF-GDC-Pr_6O_{11}	1.57	[27]
Ni-YSZ|YSZ|GDC	PBFZr-GDC	1.9	[11]
Ni-YSZ|YSZ|GDC	PBCC-GDC	1.74	[28]
Ni-YSZ|YSZ	SCP-GDC	1.4	[29]
Ni-YSZ|YSZ	PBSCF-GDC	1.37	[29]
Ni-YSZ|YSZ	MCO-GDC	0.7	[30]
Ni-YSZ|YSZ	CMO-SDC	0.64	[31]
Ni-YSZ|YSZ|SDC	BCFN/BCO-LSCF	1.4	[25]
Ni-YSZ|YSZ|GDC	BSNM-SDC-Ag	1.3	[32]
Ni-YSZ|YSZ|GDC	SSC-SDC	2.44	[1]
Ni-YSZ|YSZ|ESB	LSM-ESB	1.75	[33]
Ni-YSZ|YSZ|GDC	NBCCF@GDC	1	[34]

Table S3. XRD refinement results of the hybrid electrode material.

Sample	Phase	Space group	a, b, c (Å)	α, β, γ (°)	Wt. frac. (%)	Chi	wR_p (%)	R_p (%)	d-spacing
New PBSCF-b+BSC	New PBSCF-b	Tetragonal; P4/mmm	3.88, 3.88, 7.74	90, 90, 90	89.5	1.978	13.68	11.04	0.195 nm, (200); 0.387 nm, (002); 0.273 nm, (102); 0.158 nm, (212);
	BSC	Hexagonal; P63/mmc	5.58, 5.58, 4.63	90, 90, 120	10.5				0.279 nm, (110); 0.167 nm, (202); 0.169 nm, (211); 0.230 nm, (002);

Table S4. Comparison in peak power densities at various temperature using different single cell configuration fueled by propane.

Single cell configuration (fuel electrode| electrolyte| oxygen electrode)	Temperature (°C)	Peak power density (W cm^{-2})	Literature
Ni-YSZ|YSZ|Hybrid electrode	750	2.6	This work
	700	1.7	
	650	0.95	
	600	0.54	
	550	0.26	
RP-SFM-SDC|LDC|LSGM|LSCF-SDC	800	0.7	[35]
	750	0.35	
LSCrFeCo-GDC|LDC|LSGM|LSCF-GDC	800	0.5	[36]
	750	0.38	
	700	0.18	
L-PBMCO|LDC|LSGM|NBSCF-GDC	800	0.33	[37]
RP-PSFN-CFA|LDC|LSGM|BCFN	800	0.59	[38]
PBMO|LDC|LSGM|NBSCF-GDC	800	0.75	[39]
	750	0.3	
	700	0.17	
NTO-Ni-YSZ|YSZ|LSM-YSZ	700	0.15	[40]
BaO/Ni-YSZ|YSZ|SDC-LSCF	750	0.9	[41]
Ru-CeO2|PSZ|Ni-YSZ|YSZ|LSCF-GDC	750	0.48	[42]
	700	0.385	
PSCFN-Co-Fe|LSGM|BCFN	800	0.6	[43]
	750	0.32	
RP-PSFR-FRA-GDC|LSGM|LSCF-GDC	800	0.5	[44]
	750	0.25	
	700	0.12	

Table S5. Crystal structure results obtained from TEM for the PBSCF-b phase.

Multi.	(h,k,l)	d* / nm^{-1}	Θ_{Scatt} / Deg.	Intens.	Θ_{Bragg} / mRad	V_r [V||nm||e]	V_i [V||nm||e]	Ampli. [V||nm||e]	d / nm	LP factor	s
1	(0,0,0)	0.000	0.000		0.000	12.339	0.935	12.375			
2	(0,0,1)	1.310	0.189	1	1.642	-0.154	0.247	0.291	0.764	0.7636	1
4	(1,0,0)	2.558	0.368	301	3.208	4.917	0.479	4.940	0.391	0.3909	1
2	(0,0,2)	2.619	0.377	561	3.284	9.623	0.699	9.649	0.382	0.3818	4
8	(1,0,1)	2.874	0.413	489	3.604	4.695	0.471	4.719	0.348	0.348	2
4	(1,1,0)	3.617	0.520	1	4.536	0.249	0.256	0.357	0.276	0.2764	2
8	(1,0,2)	3.661	0.527	300	4.591	4.146	0.453	4.170	0.273	0.2731	5
8	(1,1,1)	3.847	0.553	1000	4.824	7.779	0.642	7.806	0.260	0.2599	3
2	(0,0,3)	3.929	0.565	1	4.927	0.266	0.255	0.368	0.255	0.2545	9
8	(1,1,2)	4.466	0.642	2	5.600	0.274	0.252	0.372	0.224	0.2239	6
8	(1,0,3)	4.688	0.674	167	5.879	3.497	0.430	3.523	0.213	0.2133	10
4	(2,0,0)	5.116	0.736	244	6.415	6.259	0.593	6.287	0.195	0.1955	4
2	(0,0,4)	5.238	0.753	114	6.569	6.135	0.589	6.163	0.191	0.1909	16
8	(2,0,1)	5.281	0.759	1	6.622	0.252	0.247	0.353	0.189	0.1894	5
8	(1,1,3)	5.341	0.768	434	6.697	6.034	0.585	6.062	0.187	0.1872	11
8	(2,1,0)	5.720	0.822	98	7.172	2.955	0.408	2.983	0.175	0.1748	5
8	(2,0,2)	5.747	0.826	355	7.207	5.655	0.571	5.684	0.174	0.174	8
8	(1,0,4)	5.830	0.838	93	7.310	2.904	0.405	2.932	0.172	0.1715	17
16	(2,1,1)	5.868	0.844	183	7.358	2.886	0.404	2.915	0.170	0.1704	6
16	(2,1,2)	6.291	0.904	150	7.889	2.700	0.395	2.729	0.159	0.159	9
8	(1,1,4)	6.366	0.915	1	7.983	0.197	0.242	0.312	0.157	0.1571	18
8	(2,0,3)	6.450	0.927	1	8.089	0.192	0.241	0.309	0.155	0.155	13
2	(0,0,5)	6.548	0.941	0	8.211	0.187	0.241	0.305	0.153	0.1527	25
16	(2,1,3)	6.939	0.998	111	8.702	2.444	0.387	2.474	0.144	0.1441	14
8	(1,0,5)	7.030	1.011	54	8.816	2.410	0.385	2.441	0.142	0.1422	26

Table S6. Crystal structure results obtained from TEM for the BSC phase.

Multi.	(h,k,l)	d* / nm^{-1}	Θ_{Scatt} / Deg.	Intens.	Θ_{Bragg} / mRad	V_r [V||nm||e]	V_i [V||nm||e]	Ampli. [V||nm||e]	d / nm	LP factor	s
1	(0,0,0)	0.000	0.000		0.000	28.782	2.090	28.858			
6	(1,0,0)	2.084	0.300	168	2.613	4.877	0.693	4.926	0.480	0.480	1
6	(1,1,0)	3.609	0.519	69	4.525	4.112	0.659	4.165	0.277	0.2771	2
6	(2,0,0)	4.167	0.599	1000	5.225	16.942	1.342	16.995	0.240	0.240	4
2	(0,0,2)	4.232	0.609	321	5.307	16.749	1.337	16.805	0.236	0.2363	4
12	(1,0,2)	4.717	0.678	77	5.915	3.482	0.631	3.539	0.212	0.212	5
12	(2,1,0)	5.513	0.793	51	6.913	3.060	0.610	3.121	0.181	0.1814	5
12	(1,1,2)	5.562	0.800	50	6.974	3.036	0.609	3.096	0.180	0.1798	6
12	(2,0,2)	5.939	0.854	783	7.448	12.636	1.197	12.692	0.168	0.1684	8
6	(3,0,0)	6.251	0.899	18	7.838	2.711	0.589	2.775	0.160	0.160	9
24	(2,1,2)	6.950	0.999	51	8.715	2.419	0.579	2.488	0.144	0.1439	9
6	(2,2,0)	7.218	1.038	221	9.051	10.446	1.116	10.506	0.139	0.1386	8
12	(3,1,0)	7.512	1.080	20	9.420	2.210	0.564	2.281	0.133	0.1331	10
12	(3,0,2)	7.548	1.085	20	9.466	2.197	0.563	2.268	0.132	0.1325	13
6	(4,0,0)	8.334	1.198	139	10.451	8.905	1.043	8.966	0.120	0.120	16
12	(2,2,2)	8.367	1.203	275	10.492	8.864	1.041	8.925	0.120	0.1195	12
2	(0,0,4)	8.464	1.217	44	10.614	8.743	1.034	8.804	0.118	0.1181	16
24	(3,1,2)	8.622	1.240	25	10.812	1.855	0.533	1.930	0.116	0.116	14
12	(1,0,4)	8.716	1.253	12	10.930	1.828	0.531	1.904	0.115	0.1147	17
12	(3,2,0)	9.082	1.306	10	11.389	1.728	0.521	1.805	0.110	0.1101	13
12	(1,1,4)	9.201	1.323	10	11.538	1.697	0.517	1.774	0.109	0.1087	18
12	(4,0,2)	9.347	1.344	187	11.721	7.716	0.978	7.778	0.107	0.107	20
12	(2,0,4)	9.434	1.356	181	11.830	7.622	0.973	7.684	0.106	0.106	20

12	(4,1,0)	9.548	1.373	9	11.973	1.610	0.507	1.688	0.105	0.1047	17
24	(3,2,2)	10.020	1.440	14	12.565	1.500	0.494	1.580	0.100	0.0998	17

Table S7. Summary of the stability testing results of our SOECs with the hybrid electrode

Operation	Fuel humidity	Current density	Temperature	Degradation rate
Discharging	3% humidified H_2	0.8 A cm^{-2}	650 °C	2 mV/h
	3% humidified H_2	0.2 A cm^{-2}	550 °C	1 mV/h
	3% humidified C_3H_8	0.4 A cm^{-2}	600 °C	8 mV/h
Charging	40% humidified H_2	0.8 A cm^{-2}	650 °C	3 mV/h
	40% humidified H_2	3.0 A cm^{-2}	650 °C	8 mV/h
	40% humidified H_2	5.0 A cm^{-2}	750 °C	4 mV/min

References

1 H. Shimada, T. Yamaguchi, H. Kishimoto, H. Sumi, Y. Yamaguchi, K. Nomura and Y. Fujishiro, *Nat Commun*, 2019, **10**, 5432.
2 S.-L. Zhang, H. Wang, M. Y. Lu, A.-P. Zhang, L. V. Mogni, Q. Liu, C.-X. Li, C.-J. Li and S. A. Barnett, *Energy Environ. Sci.*, 2018, **11**, 1870–1879.
3 Z. Teng, Z. Xiao, G. Yang, L. Guo, X. Yang, R. Ran, W. Wang, W. Zhou and Z. Shao, *Materials Today Energy*, 2020, **17**, 100458.
4 T. Chen, Y. Zhou, M. Liu, C. Yuan, X. Ye, Z. Zhan and S. Wang, *Electrochemistry Communications*, 2015, **54**, 23–27.
5 H. Yu, H. Im and K. T. Lee, *Adv Funct Materials*, 2022, 2207725.
6 B.-H. Yun, K. J. Kim, D. W. Joh, M. S. Chae, J. J. Lee, D. Kim, S. Kang, D. Choi, S.-T. Hong and K. T. Lee, *J. Mater. Chem. A*, 2019, **7**, 20558–20566.
7 J. H. Park, C. H. Jung, K. J. Kim, D. Kim, H. R. Shin, J.-E. Hong and K. T. Lee, *ACS Appl. Mater. Interfaces*, 2021, **13**, 2496–2506.
8 J. Kim, S. Im, S. H. Oh, J. Y. Lee, K. J. Yoon, J.-W. Son, S. Yang, B.-K. Kim, J.-H. Lee, H.-W. Lee, J.-H. Lee and H.-I. Ji, *Sci. Adv.*, 2021, **7**, eabj8590.
9 J. Yan, Z. Zhao, L. Shang, D. Ou and M. Cheng, *Journal of Power Sources*, 2016, **319**, 124–130.
10 B.-K. Park, R. Scipioni, Q. Zhang, D. Cox, P. W. Voorhees and S. A. Barnett, *J. Mater. Chem. A*, 2020, **8**, 11687–11694.
11 G. Li, Y. Gou, X. Cheng, Z. Bai, R. Ren, C. Xu, J. Qiao, W. Sun, Z. Wang and K. Sun, *ACS Appl. Mater. Interfaces*, 2021, **13**, 34282–34291.
12 K. Joong Yoon, M. Biswas, H.-J. Kim, M. Park, J. Hong, H. Kim, J.-W. Son, J.-H. Lee, B.-K. Kim and H.-W. Lee, *Nano Energy*, 2017, **36**, 9–20.
13 Z. Li, B. Yang, B. Qian, S. Wang, Y. Zheng, L. Ge and H. Chen, *Separation and Purification Technology*, 2023, **308**, 123002.
14 K. T. Bae, I. Jeong, D. Kim, H. Yu, H.-N. Im, A. Akromjon, C.-W. Lee and K. T. Lee, *Chemical Engineering Journal*, 2023, **461**, 142051.
15 T. Liu, Y. Wang, Y. Zhang, S. Fang, L. Lei, C. Ren and F. Chen, *Electrochemistry Communications*, 2015, **61**, 106–109.
16 D. Kim, J. W. Park, M. S. Chae, I. Jeong, J. H. Park, K. J. Kim, J. J. Lee, C. Jung, C.-W. Lee, S.-T. Hong and K. T. Lee, *J. Mater. Chem. A*, 2021, **9**, 5507–5521.
17 Y. Tan, A. Wang, L. Jia, D. Yan, B. Chi, J. Pu and J. Li, *International Journal of Hydrogen Energy*, 2017, **42**, 4456–4464.
18 D. Heidari, S. Javadpour and S. H. Chan, *Energy Conversion and Management*, 2017, **136**, 78–84.
19 M. A. Laguna-Bercero, H. Monzón, A. Larrea and V. M. Orera, *J. Mater. Chem. A*, 2016, **4**, 1446–1453.
20 M.-B. Choi, B. Singh, E. D. Wachsman and S.-J. Song, *Journal of Power Sources*, 2013, **239**, 361–373.
21 H.-J. Choi, Y.-H. Na, M. Kwak, T. W. Kim, D.-W. Seo, S.-K. Woo and S.-D. Kim, *Ceramics International*, 2017, **43**, 13653–13660.
22 K. J. Kim, I. Thaheem, I. Jeong, H. Yu, J. H. Park and K. T. Lee, *Journal of Power Sources*, 2022, **539**, 231611.
23 Y. Tian, W. Wang, Y. Liu, L. Zhang, L. Jia, J. Yang, B. Chi, J. Pu and J. Li, *ACS Appl. Energy Mater.*, 2019, **2**, 3297–3305.

24 Z. Yue, L. Jiang, Z. Chen, N. Ai, Y. Zou, S. P. Jiang, C. Guan, X. Wang, Y. Shao, H. Fang, Y. Luo and K. Chen, *ACS Appl. Mater. Interfaces*, 2023, **15**, 8138–8148.
25 Y. Niu, Y. Zhou, W. Lv, Y. Chen, Y. Zhang, W. Zhang, Z. Luo, N. Kane, Y. Ding, L. Soule, Y. Liu, W. He and M. Liu, *Adv. Funct. Mater.*, 2021, **31**, 2100034.
26 B.-K. Park and S. A. Barnett, *J. Mater. Chem. A*, 2020, **8**, 11626–11631.
27 X. Tong, Y. Xu, Đ. Tripković, P. V. Hendriksen, W.-R. Kiebach and M. Chen, *J. Mater. Chem. A*, 2020, **8**, 9039–9048.
28 Z. Chen, L. Jiang, S. He, C. Guan, Y. Zou, Z. Yue, N. Ai, S. P. Jiang, Y. Shao and K. Chen, *Applied Catalysis B: Environmental*, 2022, **305**, 121056.
29 K. Chen, N. Li, N. Ai, M. Li, Y. Cheng, W. D. A. Rickard, J. Li and S. P. Jiang, *J. Mater. Chem. A*, 2016, **4**, 17678–17685.
30 H. Liu, X. Zhu, M. Cheng, Y. Cong and W. Yang, *Chem. Commun.*, 2011, **47**, 2378–2380.
31 L. Zhang, D. Li and S. Zhang, *Ceramics International*, 2017, **43**, 2859–2863.
32 Y. Zhu, W. Zhou, Y. Chen and Z. Shao, *Angew. Chem. Int. Ed.*, 2016, **55**, 8988–8993.
33 Y. Liu, Y. Tian, W. Wang, Y. Li, S. Chattopadhyay, B. Chi and J. Pu, *ACS Appl. Mater. Interfaces*, 2020, **12**, 57941–57949.
34 Y. Tian, W. Wang, Y. Liu, A. Naden, M. Xu, S. Wu, B. Chi, J. Pu and J. T. S. Irvine, *ACS Catal.*, 2021, **11**, 3704–3714.
35 X. Xi, Z.-S. Cao, X.-Q. Shen, Y. Lu, J. Li, J.-L. Luo and X.-Z. Fu, *Journal of Power Sources*, 2020, **459**, 228071.
36 K.-Y. Lai and A. Manthiram, *Chem. Mater.*, 2018, **30**, 2515–2525.
37 O. Kwon, S. Sengodan, K. Kim, G. Kim, H. Y. Jeong, J. Shin, Y.-W. Ju, J. W. Han and G. Kim, *Nat Commun*, 2017, **8**, 15967.
38 C. Yang, J. Li, Y. Lin, J. Liu, F. Chen and M. Liu, *Nano Energy*, 2015, **11**, 704–710.
39 S. Sengodan, S. Choi, A. Jun, T. H. Shin, Y.-W. Ju, H. Y. Jeong, J. Shin, J. T. S. Irvine and G. Kim, *Nature Mater*, 2015, **14**, 205–209.
40 Z. Wang, Z. Wang, W. Yang, R. Peng and Y. Lu, *Journal of Power Sources*, 2014, **255**, 404–409.
41 L. Yang, Y. Choi, W. Qin, H. Chen, K. Blinn, M. Liu, P. Liu, J. Bai, T. A. Tyson and M. Liu, *Nat Commun*, 2011, **2**, 357.
42 Z. Zhan and S. Barnett, *Solid State Ionics*, 2005, **176**, 871–879.
43 L. Zhang, C. Yang, A. I. Frenkel, S. Wang, G. Xiao, K. Brinkman and F. Chen, *Journal of Power Sources*, 2014, **262**, 421–428.
44 M. Qin, T. Tan, K. Li, Z. Wang, H. Yang, Z. Liu, M. Zhou, T. Liu, C. Yang and M. Liu, *International Journal of Hydrogen Energy*, 2020, **45**, 21464–21472.